PGC1α/β Expression Predicts Therapeutic Response to Oxidative Phosphorylation Inhibition in Ovarian Cancer

Carmen Ghilardi[1], Catarina Moreira-Barbosa[1,2], Laura Brunelli[3], Paola Ostano[4], Nicolò Panini[5], Monica Lupi[5], Alessia Anastasia[1], Fabio Fiordaliso[6], Monica Salio[6], Laura Formenti[1,7], Massimo Russo[1], Edoardo Arrigoni[7], Ferdinando Chiaradonna[7], Giovanna Chiorino[4], Giulio Draetta[8,9,10], Joseph R. Marszalek[9], Christopher P. Vellano[9], Roberta Pastorelli[3], MariaRosa Bani[1], Alessandra Decio[1], and Raffaella Giavazzi[1]

ABSTRACT

Ovarian cancer is the deadliest gynecologic cancer, and novel therapeutic options are crucial to improve overall survival. Here we provide evidence that impairment of oxidative phosphorylation (OXPHOS) can help control ovarian cancer progression, and this benefit correlates with expression of the two mitochondrial master regulators PGC1α and PGC1β. In orthotopic patient-derived ovarian cancer xenografts (OC-PDX), concomitant high expression of PGC1α and PGC1β (PGC1α/β) fostered a unique transcriptional signature, leading to increased mitochondrial abundance, enhanced tricarboxylic acid cycling, and elevated cellular respiration that ultimately conferred vulnerability to OXPHOS inhibition. Treatment with the respiratory chain complex I inhibitor IACS-010759 caused mitochondrial swelling and ATP depletion that consequently delayed malignant progression and prolonged the lifespan of high PGC1α/β-expressing OC-PDX-bearing mice. Conversely, low PGC1α/β OC-PDXs were not affected by IACS-010759, thus pinpointing a selective antitumor effect of OXPHOS inhibition. The clinical relevance of these findings was substantiated by analysis of ovarian cancer patient datasets, which showed that 25% of all cases displayed high PGC1α/β expression along with an activated mitochondrial gene program. This study endorses the use of OXPHOS inhibitors to manage ovarian cancer and identifies the high expression of both PGC1α and β as biomarkers to refine the selection of patients likely to benefit most from this therapy.

Significance: OXPHOS inhibition in ovarian cancer can exploit the metabolic vulnerabilities conferred by high PGC1α/β expression and offers an effective approach to manage patients on the basis of PGC1α/β expression.

Introduction

Metabolic adaptation has emerged as a hallmark of cancer (1) and confers growth advantages to tumors. Cancer cells present a mixed energy phenotype. Although aerobic glycolysis is often found, oxidative phosphorylation (OXPHOS) contributes to energy production, with a major role in some tumors (2). OXPHOS occurs in mitochondria and fuels cancer cells, using a variety of substrates. By oxidizing pyruvate, fatty acid, and amino acids through the tricarboxylic acid (TCA) cycle, mitochondria generate the reducing equivalent (NADH, FADH2) for fueling the electron transport chain (ETC) and producing ATP and biosynthetic molecules that support tumor cell proliferation.

The importance of OXPHOS in ovarian cancer has been recently highlighted. Mitochondrial DNA content strongly correlated with the expression of genes involved in the ETC and TCA cycle (3) and was significantly higher in ovarian carcinoma cells than in normal ovary (4). Using The Cancer Genome Atlas database, Yang and colleagues reported that the poor survival of ovarian cancer patients significantly correlated with high expression levels of genes involved in glutaminolysis or the TCA cycle and low expression of glycolysis-related genes (5). High expression of a "Mito-signature," including transcripts of OXPHOS complexes, significantly predicted tumor recurrence, progression, and reduced overall survival of ovarian cancer patients (6). Highly invasive ovarian cancer cells preferentially use glutamine rather than glucose to replenish the TCA cycle, dramatically raising the oxygen consumption rate. Interfering with OXPHOS metabolism by mitochondrial respiratory complex I inhibition (e.g., rotenone) reduces both the TCA cycle activity and ovarian cancer cell invasiveness (5). OXPHOS also appears to play a key role in the insurgence of chemoresistance (7–10), which has a heavy impact on patient survival,

[1]Laboratory of Cancer Metastasis Therapeutics, Istituto di Ricerche Farmacologiche Mario Negri IRCCS, Milan, Italy. [2]Institute of Biomedical Sciences Abel Salazar (ICBAS), University of Porto, Porto, Portugal. [3]Laboratory of Mass Spectrometry, Istituto di Ricerche Farmacologiche Mario Negri IRCCS, Milan, Italy. [4]Cancer Genomics Laboratory, Fondazione Edo ed Elvo Tempia Valenta, Biella, Italy. [5]Laboratory of Anticancer Pharmacology, Istituto di Ricerche Farmacologiche Mario Negri IRCCS, Milan, Italy. [6]Laboratory of Cardiovascular Clinical Pharmacology, Istituto di Ricerche Farmacologiche Mario Negri IRCCS, Milan, Italy. [7]Department of Biotechnology and Biosciences, University of Milano-Bicocca, Milan, Italy. [8]Institute for Applied Cancer Science, Therapeutics Discovery Division, The University of Texas MD Anderson Cancer Center, Houston, Texas. [9]TRACTION Platform, Therapeutics Discovery Division, The University of Texas MD Anderson Cancer Center, Houston, Texas. [10]Department of Genomic Medicine, The University of Texas MD Anderson Cancer Center, Houston, Texas.

Note: Supplementary data for this article are available at Cancer Research Online (http://cancerres.aacrjournals.org/).

C. Ghilardi and C. Moreira-Barbosa contributed equally to this article.

M. Bani, A. Decio, and , R. Giavazzi contributed equally to this article.

Corresponding Author: Carmen Ghilardi, Department of Oncology, Laboratory of Cancer Metastasis Therapeutics; Istituto di Ricerche Farmacologiche Mario Negri IRCCS, Via Mario Negri 2, 20156 Milan, Italy. Phone: 39-02-39014226; Fax: 39-02-39014734; E-mail: carmen.ghilardi@marionegri.it

Cancer Res 2022;82:1423–34

doi: 10.1158/0008-5472.CAN-21-1223

and in the maintenance of ovarian cancer stem cells (CSC). These cells, with high metastatic and tumorigenic potential, are more reliant on OXPHOS to support stemness and their high energy-consuming functions, such as proliferation, growth, migration, and invasion. Ovarian CSCs show increased expression of genes involved in glucose uptake, OXPHOS metabolism, and fatty acid beta-oxidation (11). All these pieces of evidences suggest that targeting OXPHOS could be a promising therapeutic avenue to delay ovarian cancer progression and, possibly, to eliminate residual disease.

Searching for reliable markers to define the dependence on OXPHOS, we focused on the peroxisome proliferator-activated receptor gamma coactivator 1-alpha and beta (PGC1α and PGC1β; ref. 12). PGC1α has emerged as a master regulator of mitochondrial biogenesis and energy expenditure and is important in the adaptive metabolic response. PGC1β is responsible for basal mitochondrial functions (13). PGC1α and PGC1β both have functions that favor carcinogenesis and progression in some cancer types (14) and promote metastasis (15). However, their role in tumor development is tissue-dependent and still debated (14, 16).

Here we investigated the expression of PGC1α and PGC1β in ovarian cancer patients and patient-derived xenografts (OC-PDX) and found it closely correlated with OXPHOS activity and the mitochondrial metabolism of cancer cells. In a subset of OC-PDXs, we also demonstrated that their high expression strongly correlates with the therapeutic response to IACS-010759, an OXPHOS inhibitor that targets complex I of the ETC (17).

Materials and Methods

Animals

Six- to eight-week-old female athymic Nude-*Foxn1*^{nu} mice were obtained from Envigo Laboratories. Mice were maintained under specific-pathogen-free conditions, housed in isolated vented cages, and handled using aseptic procedures. Animal studies were approved by the Mario Negri Institute Animal Care and Use Committee and the Italian Ministry of Health. Procedures involving animals and their care were conducted in conformity with the laws, regulations, and policies governing the care and use of laboratory animals—Italian Governing Law (D.lgs 26/2014, authorization number 19/2008-A issued March 6, 2008, by the Ministry of Health); providing internal authorization for people conducting animal experiments (Quality Management System Certificate—UNI EN ISO9001: 2008—registration number 6121); the NIH Guide for the Care and Use of Laboratory Animals (2011 edition); and EU directives and guidelines (EEC Council Directive 2010/63/UE)—and were in line with guidelines for the welfare and use of animals in cancer research (18).

Orthotopic xenograft tumor models

Seven OC-PDX (Y-HOC8, HOC10, HOC22, HOC76, HOC78, HOC79, and HOC84) were molecularly, biologically, and pharmacologically characterized, and previously described (19, 20). OC-PDXs were propagated by collection of malignant ascites and intraperitoneal (i.p.) transplantation in nude mice as a tumor suspension of 10×10^6 cells. Tumor growth was evaluated on the basis of abdominal distension and palpable tumor masses in the peritoneal cavity (19).

Pharmacologic treatment

OC-PDX-bearing mice were randomized (simple randomization; 10–15 per group) on the day specified in the figure legends, and groups were arbitrarily assigned to receive either IACS-010759 or vehicle. IACS-010759 (provided by MD Anderson Cancer Center Institute for Applied Cancer Science) was dissolved in 0.5% methylcellulose (Sigma-Aldrich) and administered by gavage 5 days on/2 off at 2.5 mg/kg, in a maintenance regimen (unless otherwise specified). Vehicle was given with the same schedule as the active drug. Mice were monitored daily and were euthanized when they presented signs of distress due to disease progression (visible abdominal swelling, hemorrhagic ascites, and palpable abdominal tumor masses). The time-to-disease progression (day of sacrifice) was recorded as survival time (ST) to generate Kaplan–Meier curves. The increment of lifespan (ILS) was calculated as $100 \times [(\text{median survival day}_{\text{treated group}} - \text{median survival day}_{\text{control group}})/\text{median survival day}_{\text{control group}}]$.

At necropsy, malignant ascites were harvested, and the volume of cells was recorded to evaluate the abdominal tumor burden.

In vivo oxygen consumption and lactate release

OC-PDX ascites were harvested and centrifuged at 1,200 rpm for 10 minutes. Cell pellets were resuspended in HBSS medium (Thermo Fisher Scientific) and immediately transferred to the Clark oxygen electrode chamber (Hansatech). The oxygen consumption rate (OCR) was measured over a time course, and the values were normalized to the total protein content. Cell-free supernatants were analyzed for lactate concentration with the Vi-CELL MetaFLEX ANALYZER (Beckman Coulter). Each sample was analyzed in triplicate.

In vivo ^{13}C6-glucose tracing

OC-PDX-bearing mice were injected intraperitoneally with 1 g/kg $^{13}C_6$-glucose (Cambridge Isotopes Laboratories), and after 30 minutes, cells from ascites were collected, rinsed, and their metabolism quenched with liquid nitrogen. Metabolites were extracted and analyzed by liquid chromatography high resolution–mass spectrometry as described (21). Details are reported in Supplementary Methods.

Mitochondrial ultrastructure, number, and volume assessment

Cells from malignant ascites were centrifuged, washed with phosphate buffer (0.12M), and prepared for transmission electron microscopy (TEM), as previously described (22). Details are reported in Supplementary Methods.

ATP measurement

Total proteins were extracted with passive lysis buffer (Promega) and quantified using the Bio-Rad Bradford protein assay. Intracellular ATP levels were measured with the ATP determination kit (Molecular Probes). The luminescent signal was measured in a GloMax Discover Microplate Reader (Promega). Each sample was analyzed in triplicate.

Gene expression data analysis

MeV version 4.9.0 was used for unsupervised hierarchical clustering on the gene expression profiling from ovarian cancer patients and OC-PDX. Pearson/Cosine distance was used as similarity metric and average linkage as the linkage method. Overrepresented biological processes of Gene Ontology (GO) were investigated with the functional annotation tool available in DAVID 6.8 (https://david.ncifcrf.gov/, RRID:SCR_001881). Correlation analysis was done with the cor and cor.test functions, available in the R statistical environment, using Pearson correlation. Genes with Pearson $r > 0$ and $P < 0.01$ were considered positively correlated to both PGC1α and PGC1β.

RT-qPCR

TotRNA was isolated using a miRNEasy mini kit (QIAGEN) and retrotranscribed (1 μg) using the High-Capacity cDNA Reverse Transcription Kit (Applied Biosystems). The gene expression levels were measured by qPCR using TaqMan Universal PCR Master Mix (Applied Biosystems) and specific TaqMan Gene Expression Assays (IDT). Expression levels were normalized to β-actin and presented as relative expression ($2^{(-DDCt)}$). The samples were run in triplicate.

Western blot

Nuclear proteins were extracted using NE-PER nuclear and cytoplasmic extraction reagents (Thermo Fisher Scientific) with protease inhibitors (Roche). Ten μg of proteins was separated onto precast 4% to 12% polyacrylamide gels (Sigma-Aldrich) and transferred to 0.2-μm PVDF membranes using a trans-blot turbo system (Bio-Rad). Blots were blocked at room temperature for 2 hours in blocking buffer [5% nonfat dry milk or 5% BSA in TBS/0.1% Tween 20 (Sigma-Aldrich)], then incubated overnight at 4°C with the appropriate primary antibody: PGC1α (1:1,000, Novus Biologicals; cat. #NBP1-04676, RRID: AB_1522118), PGC1β (1:10,000, Abcam; cat. #ab176328, RRID: AB_2893194), Histone H3 (1:2,000, Abcam; cat. #ab1791, RRID: AB_302613). Antibody binding was detected using anti-rabbit IgG-HRP (1:5,000, Sigma-Aldrich; cat. #A6154, RRID:AB_258284) for 1 hour at room temperature. The signals were revealed with ECL (Thermo Fisher Scientific) and acquired with an Odyssey Fc Imaging System. Histone H3 was used for normalization.

Cell culture

OVCAR3 (NCI-DTP; cat. #OVCAR3, RRID:CVCL_0465) and IGROV1 (NCI-DTP; cat. #IGR-OV1, RRID:CVCL_1304) human ovarian adenocarcinoma cells were obtained from the NCI (Fredrick, MD) and were routinely cultured in RPMI-1640 medium (Microgem) supplemented with 10% FBS (Microgem) and 2 mmol/L L-glutamine (GIBCO). Stocks of cell lines, authenticated by short-tandem repeat profiling (AmpFlSTR Identifiler Plus PCR Amplification Kit; Applied Biosystems), were stored frozen in liquid nitrogen and used within 4 weeks after thawing. Cells were routinely tested for *Mycoplasma* contamination by PCR.

Generation of PGC1α and PGC1β knockout cells

To generate syngeneic PGC1α and PGC1β knockout (KO) cells, 2 μg of gene-specific CRISPR/Cas9 KO plasmid was cotransfected with 2 μg of the corresponding HDR plasmid into 1×10^6 OVCAR3 cells by way of Amaxa Nucleofector Technology (Nucleofector kit V, Program T-016). The following plasmids, purchased from SantaCruz Biotechnology, were used: PGC1α CRISPR/Cas9 KO (sc-400070), PGC1α HDR (sc-400070-HDR), PGC1β KO CRISPR/Cas9 (sc-417930), and PGC1β HDR (sc-417930-HDR). Selection of transfected cells was performed 72 hours later with 5 μg/mL puromycin. Individual clones were then isolated by mechanical detachment of single colonies and further expanded for characterization. Gene silencing was verified evaluating the protein levels by western blot. Cells transfected with the same plasmids, in which PGC1α and PGC1β were not successfully silenced, were used as control cells (ctr-KO OVCAR3).

Cellular reactive oxygen species and MitoTracker staining

Cells were stained with 5 μmol/L CellROX Deep Red reagent (Invitrogen) for 30 minutes at 37°C for reactive oxygen species (ROS) quantification or with 25 nmol/L MitoTracker Deep Red (Invitrogen) for 45 minutes at 37°C for the determination of mitochondrial content. Data were acquired on a Gallios flow cytometer (Beckman Coulter) and analyzed using Kaluza software (GalliosTM Kaluza, RRID: SCR_016700).

Seahorse analysis

50,000 cells/well were seeded in XFe96 Cell Culture Microplates (Agilent Technologies) in culture medium and incubated for 24 hours at 37°C in 5% CO_2. Before the experiment, the culture medium had been replaced with serum-free unbuffered Seahorse XF RPMI Medium pH 7.4 supplemented with 10 mmol/L glucose, 2 mmol/L glutamine, and 1 mmol/L sodium pyruvate, and then the microplate was incubated at 37°C in a non-CO_2 incubator for 1 hour. The MitoStress Test was performed. The concentrations of oligomycin, FCCP, and rotenone/antimycin A used in the assay were, respectively, 1, 0.25, and 1 μmol/L. The OCR was evaluated over a time course before and after injection of the drugs. OCR data (pmol/min/prot/mitochondrial mass) were normalized by mitochondrial mass (MitoTracker Green FM staining) and by protein amount.

Cell treatment and viability assay

4×10^3 cells/well were seeded in 96-well plates in RPMI-1640 with 2.5% FBS and 2 mmol/L glutamine. After 48 hours, the cells were treated with IACS-010759 at the concentrations indicated and cell proliferation measured after 96 hours with CellTiter 96 AQueous One Solution Cell Proliferation Assay (Promega) or crystal violet staining. Proliferation was calculated as a percentage, comparing IACS-010759–treated to vehicle-treated cells. To compare the different clones, 7.5×10^3 cells/well were plated in 24-well plates and treated with 1,000 nmol/L IACS-010759. After 96 hours, proliferation was quantified by cell count using the Coulter Counter (Beckman Coulter).

Apoptosis evaluation

OVCAR3 and IGROV1 were treated with 1,000 nmol/L IACS-010759 and collected after 24, 48, and 72 hours. Apoptosis was evaluated using the eBioscience Annexin V-FITC Apoptosis Detection Kit.

Statistical analysis

Statistical analyses were done with GraphPad Prism 7.0 software (GraphPad Software Inc., RRID:SCR_002798). The tests used are indicated in the figure legends.

Data availability statement

The data generated in this study are available within the article and its supplementary data files. Expression profile data analyzed in this study were obtained from Gene Expression Omnibus at GSE49997 and GSE56920.

Results

PGC1α and PGC1β expression stratifies ovarian cancer subsets and distinguishes tumors with OXPHOS signature

PGC1α and PGC1β expression was investigated in 204 ovarian cancer patient samples for which transcriptomic profiles were publicly available (GSE49997; ref. 23). The expression of PGC1α and PGC1β (encoded by *PPARGC1A* and *PPARGC1B*, respectively) distinguished four equally distributed subsets (**Fig. 1A**; Supplementary Table S1): high or low levels of both transcripts, high PGC1α but low PGC1β, and high PGC1β but low PGC1α. These results were reproduced in three other independent datasets comprising an additional 775 ovarian cancer cases (Supplementary Table S1), confirming that they are representative of the clinical situation. PGC1α and PGC1β expression

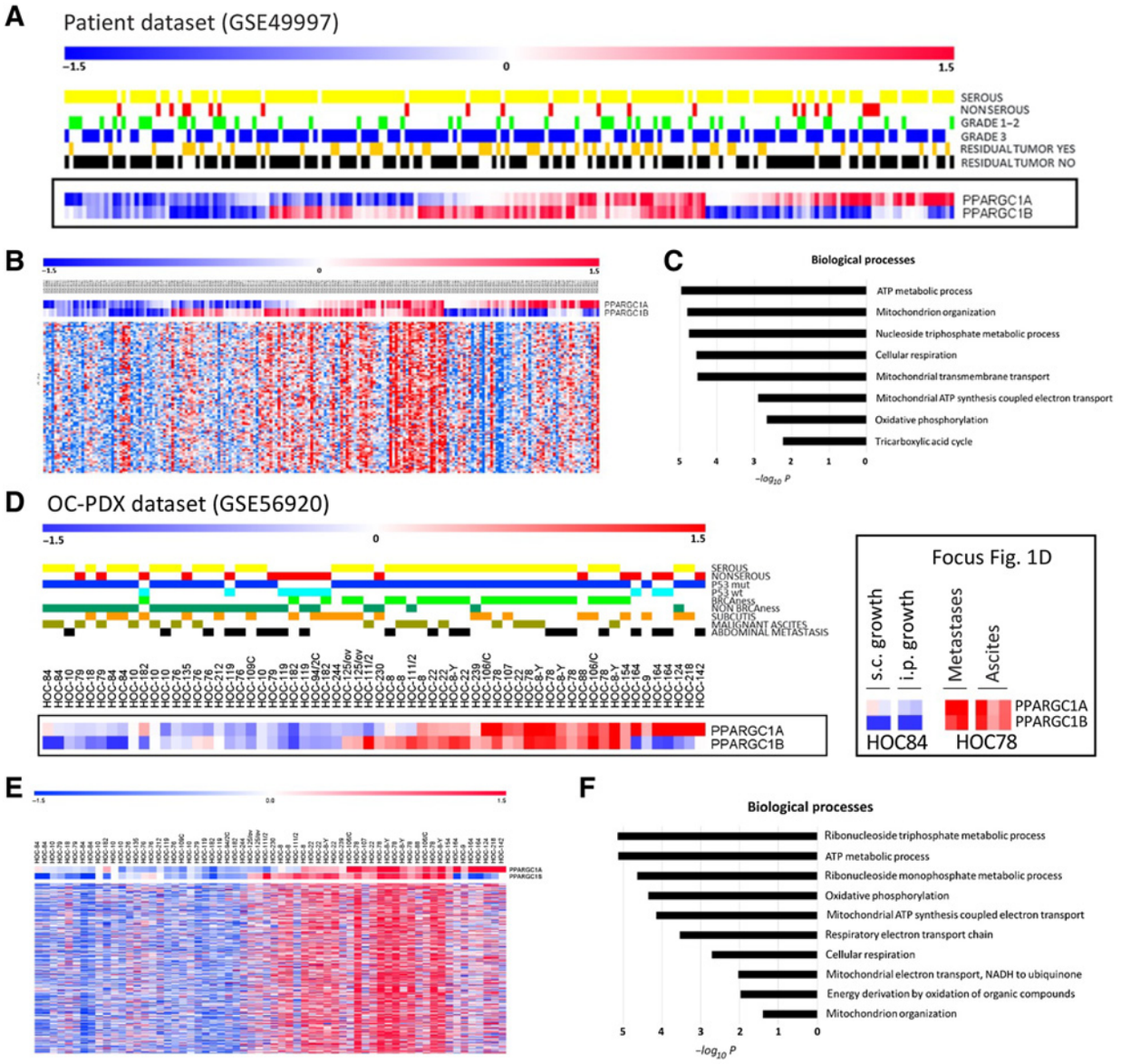

Figure 1.

PGC1α and PGC1β identify ovarian cancer with OXPHOS signature. **A,** Heatmap of PGC1α and PGC1β expression in ovarian cancer patients ($n = 204$) from the GSE49997 dataset. **B,** Heatmap of genes positively correlated with PGC1α and PGC1β expression in patients. Each column is one patient sample, and each row is the expression of each gene, expressed as Z-score, ranging from low (−1.5) to high (1.5). **C,** The biological processes enriched in patients with high PGC1α and PGC1β expression. Pathway enrichment was defined from GO, and the Benjamini–Hochberg test was used to account for multiple testing. **D,** Heatmap of PGC1α and PGC1β expression in our OC-PDX cohort (GSE56920 dataset; ref. 20) comprising 29 OC-PDX (62 samples). The samples included biological replicates from different mice and different anatomical locations: OC-PDX growing subcutaneously (s.c.) or intraperitoneally (i.p.) as malignant ascites (pea) or abdominal metastasis (mc). Each column is a xenograft sample, and each row is expression of each gene expressed as Z-score ranging from low (−1.5) to high (1.5). The focus reports PGC1α and PGC1β expression in tumors growing ectopically or orthotopically (e.g., HOC84, s.c. vs. i.p.) or as cell suspension of solid masses (e.g., HOC78, pea vs. mc). **E,** Heatmap of genes positively correlated with PGC1α and PGC1β expression in xenografts. **F,** The biological processes enriched in OC-PDX models expressing high levels of PGC1α and PGC1β.

did not correlate with any of the clinical features, tumor histotype (serous or not), grade (1, 2, or 3) or residual tumor (**Fig. 1A**), or with progression-free or overall survival.

The concomitant high expression of PGC1α and PGC1β positively correlated with the high expression of a number of genes (**Fig. 1B**; Supplementary Table S2A) belonging to biological processes related to ETC and ATP synthesis (*NDUFAB1*, *NDUFS1*, *CYCS*, *COX6A1*, *COX7C*, *ATP5L*, *ATP5H*, *ATP5I*, and *ATP5O*), the TCA cycle (*PDHA1*, *SDHC*, *OGDHL*, and *FH*), mitochondrion organization (*IMMT* and *CHCHD3*), and mitochondrial transmembrane transport system (*TIMM17A*, *TIMMB8*, and *TOMM40*, *PNPT1*, and *VDAC1*; **Fig. 1C**; Supplementary Table S2B).

Likewise, PGC1α and PGC1β expression levels classified our ovarian cancer patient-derived xenografts (OC-PDX) in four groups. PGC1α and PGC1β were simultaneously highly expressed in 10 of 29 OC-PDXs, but were detected at low levels in 12; four OC-PDXs expressed high PGC1α but low PGC1β, and 3 expressed high PGC1β and low PGC1α (**Fig. 1D**). PGC1α and PGC1β expression was an intrinsic characteristic of each OC-PDX and did not change whether the tumors were growing in an ectopic or orthotopic site (e.g., OC-PDX HOC84; focus in **Fig. 1D**), or as malignant ascites or abdominal metastasis (e.g., OC-PDX HOC78; focus in **Fig. 1D**).

As demonstrated for the patients' tumors, the concomitant high expression of PGC1α and PGC1β correlated with the enhanced expression of several genes involved in OXPHOS and mitochondrial metabolism (**Fig. 1E**; Supplementary Table S3). The overrepresented biological processes (**Fig. 1F**; Supplementary Table S4) paralleled those characterizing the clinical samples, comprising the respiratory chain (*NDUFA3*, *NDUFA5*, and *NDUFB11*; *CYC1*, *COX7b*, and *COX4I1*), ATP synthesis (*ATP5J2* and *ATP5I*), and mitochondrion organization (*CHCHD3*, *ECSIT*, *RPL28*, *MRPL21*, and *SLC25A33*). PGC1α/β expression also correlated with genes involved in glutamate biosynthesis (*GLS2* and *ALDH4A1*) and in the redox balance (*PARK7*).

These results suggest that the high expression of both PGC1α and PGC1β identifies an overactivated mitochondrial gene program characterizing approximately 25% of the tumors from ovarian cancer patients, in accordance with the findings from a cohort of OC-PDX.

High PGC1α/β expression identifies ovarian cancers with oxidative metabolism

The metabolic phenotypes associated with the simultaneous high or low expression of PGC1α and PGC1β (hereafter termed PGC1α/β) were investigated in selected OC-PDXs: HOC22, Y-HOC8, and HOC78 expressing high levels of PGC1α/β and HOC10, HOC76, HOC79, and HOC84 expressing low levels (**Fig. 2A**; Supplementary Fig. S1A).

Expression of glycolysis-related genes (e.g., *GLUT1*, *HK*, and *LDHA*) was comparable between high and low PGC1α/β expressing OC-PDXs (**Fig. 2B**), with similar amounts of lactate released in the ascites (**Fig. 2C**). Conversely, high PGC1α/β xenografts overexpressed pyruvate dehydrogenase *PDHA*, which converts pyruvate to acetyl-CoA and initiates the TCA cycle, as well as components of the respiratory chain complexes [complex I *NDUFA3*, complex II succinate dehydrogenase complex subunit C (*SDHC*), complex III cytochrome C1 (*CYC1*), and ATP synthase *ATP5I*]. High PGC1α/β levels were also associated with increased expression of the antioxidant superoxide dismutase 1 (*SOD1*), responsible for destroying free superoxide radicals, by-products of mitochondrial respiration, and of glutaminase (*GLS*), involved in the synthesis of glutathione (**Fig. 2B**). These results suggest that the genes involved in OXPHOS and detoxification of its by-products might be transcriptionally regulated by PGC1α/β.

Further, PGC1α/β expression also correlated with higher levels of genes involved in mitochondrial biogenesis (e.g., *NRF1* and *TFAM*; **Fig. 2B**). In accordance, TEM indicated that mitochondria were smaller but 75% more abundant in high PGC1α/β-expressing OC-PDXs than the low PGC1α/β OC-PDXs (**Fig. 2D**; Supplementary Fig. S1B). This was confirmed by MitoTracker staining and FACS analysis (Supplementary Fig. S1C). Consistent with these results, high PGC1α/β OC-PDXs had higher OCR than low-expressing OC-PDXs (**Fig. 2E**).

To investigate to what extent these features were related to functional alterations of the central cellular metabolism, we tracked the intracellular fate of glucose, one of the main carbon sources for cell metabolism. Mice bearing HOC22, Y-HOC8 (high PGC1α/β), and HOC10, HOC84 (low PGC1α/β) were injected i.p. with ^{13}C-glucose and the isotopologs' distribution of 13-carbon incorporation in the downstream metabolites was assessed. M + 3 pyruvate levels were significantly lower in the high PGC1α/β cells (**Fig. 3A**). High and low PGC1α/β OC-PDXs showed no major differences in M + 3 lactate and alanine production, indicating that pyruvate was diverted not to lactate fermentation or alanine transamination, but to fuel mitochondrial oxidative metabolism (**Fig. 3B**). Glucose-derived isotopolog distribution of all TCA intermediates (citrate, succinate, fumarate, and malate) showed significantly higher levels in the high PGC1α/β OC-PDXs (**Fig. 3C**). The elevated TCA cycling characterizing the high PGC1α/β OC-PDXs was reflected in significant increases in all the isotopolog fractions (M + 2, M + 3, and M + 4) of intermediates as well as of metabolites derived from the former part of the TCA cycle, such as glutamate, and glutamine, compared with the low PGC1α/β OC-PDXs (**Fig. 3D**). There were no differences in aspartate generated from the latter part of the TCA cycle (**Fig. 3D**) between high and low PGC1α/β OC-PDXs. The TCA biosynthetic flow was directed to the generation of glutamine and glutathione (GSH) whose levels were significantly higher in the high PGC1α/β OC-PDXs than in the low PGC1α/β OC-PDXs (**Fig. 3E**).

These results demonstrate that high expression of PGC1α/β distinguishes OC-PDXs bearing a distinct metabolic profile with higher mitochondrial oxidative activity.

PGC1α and PGC1β regulate OXPHOS in ovarian cancer cells

The cause–effect relationship between PGC1α/β expression and OXPHOS phenotype was investigated *in vitro*. OVCAR3 and IGROV1 cell lines were selected as representative of high or low PGC1α/β expression. OVCAR3 expressed significantly higher levels of both transcripts and proteins than IGROV1 (**Fig. 4A**), and presented features of high oxidative metabolism, as demonstrated for the OC-PDXs. OVCAR3 cells expressed higher levels of genes encoding the ETC complexes, such as *NDUFA3*, *COX7B*, *CYCS*, *SDHC*, and *ATP5I*, as well as of isocitrate dehydrogenase (*IDH1*), glutamine synthase (*GLUL*), and the glutamine transporter *SLC1A5* (**Fig. 4B**). OVCAR3 contained more mitochondria and produced more ROS than IGROV1 (**Fig. 4C**). Functionally, OVCAR3 had a higher OCR, as well as greater maximal and spare respiratory capacity than IGROV1 (**Fig. 4D**), confirming higher OXPHOS activity in high PGC1α/β cells.

To prove the cause-to-effect linking PGC1α/β expression to elevated OXPHOS metabolism, we generated isogenic PGC1α and PGC1β KO OVCAR3 cells (PGC1α-KO OVCAR3 and PGC1β-KO OVCAR3). Although complete KO was not obtained, at least 50% silencing was reached (**Fig. 4E**). PGC1α and PGC1β silencing caused downregulation of OXPHOS-related genes, particularly those involved in the ETC (*CYCS*, *CYC1*, and *COXB7* and *ATP5I*; **Fig. 4F**). Seahorse analysis showed that basal OCR, maximal, and spare respiration were significantly reduced as a consequence of PGC1α and PGC1β depletion compared with parental and ctr-KO OVCAR3 cells (**Fig. 4G**). This result implies that PGC1α and PGC1β functionally regulate OXPHOS activity of OC.

High PGC1α/β expression correlates with better responsiveness to OXPHOS inhibition

We next investigated whether PGC1α/β expression levels influenced the susceptibility of ovarian cancer cells to OXPHOS

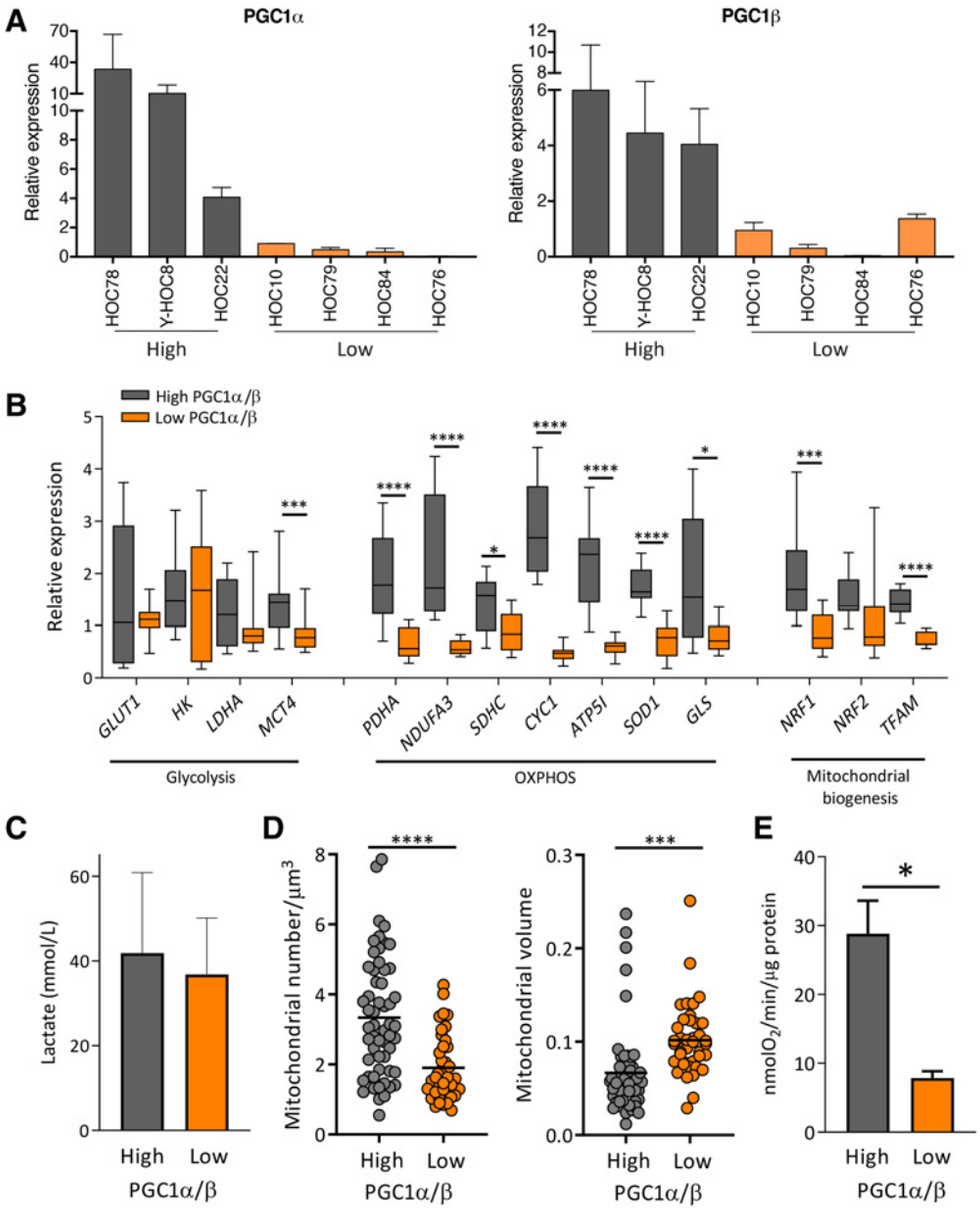

Figure 2.

PGC1α and PGC1β expression is associated with an OXPHOS phenotype. **A,** PGC1α and PGC1β transcript expression in cell aggregates from malignant ascites from OC-PDXs (mean ± SD). **B,** Expression of glycolysis, mitochondrial biogenesis, and OXPHOS-related genes in cell aggregates from malignant ascites of high or low PGC1α/β expressing OC-PDXs (median with range). **C,** Lactate concentration in the supernatant of malignant ascites (mean ± SD). **D,** Mitochondrial content and mitochondrial volume in high PGC1α/β HOC22 or low-expressing HOC10, measured by TEM. **E**, Oxygen consumption (mean ± SD) in the high PGC1α/β Y-HOC8 vs. the low-expressing HOC10. *, $P < 0.05$; ***, $P < 0.001$; ****, $P < 0.0001$, unpaired *t* test. At least three biological replicates were examined for each OC-PDX.

inhibition. To affect OXPHOS we used IACS-010759 (17), a recently developed, potent and selective small-molecule inhibitor of complex I of the mitochondrial ETC. IACS-010759 binds and inhibits the ubiquinone channel, blocking the activity of the complex I and thus OXPHOS. Preclinical studies showed that IACS-010759 is effective on acute myeloid leukemia and brain tumors addicted to OXPHOS (17).

IACS-010759 significantly impaired the proliferation of high PGC1α/β OVCAR3 cells in a dose-dependent manner, starting from the 1 nmol/L dose. IGROV1 cell growth was not significantly affected up to 10 μmol/L IACS-010759 (**Fig. 4H** and **I**). Annexin V staining showed that OXPHOS inhibition by IACS-010759 induced apoptosis in OVCAR3, but not IGROV1 cells (Supplementary Fig. S2). Further proving the functional relationship between PGC1α and PGC1β and sensitivity to OXPHOS inhibition, IACS-010759 poorly affected the proliferation of PGC1α-KO and PGC1β-KO cells, similarly to low PGC1α/β IGROV1 cells and contrarily to ctr-KO and parental OVCAR3 (**Fig. 4J** and **K**). These results indicate that PGC1α and PGC1β are functionally implicated in the response to OXPHOS

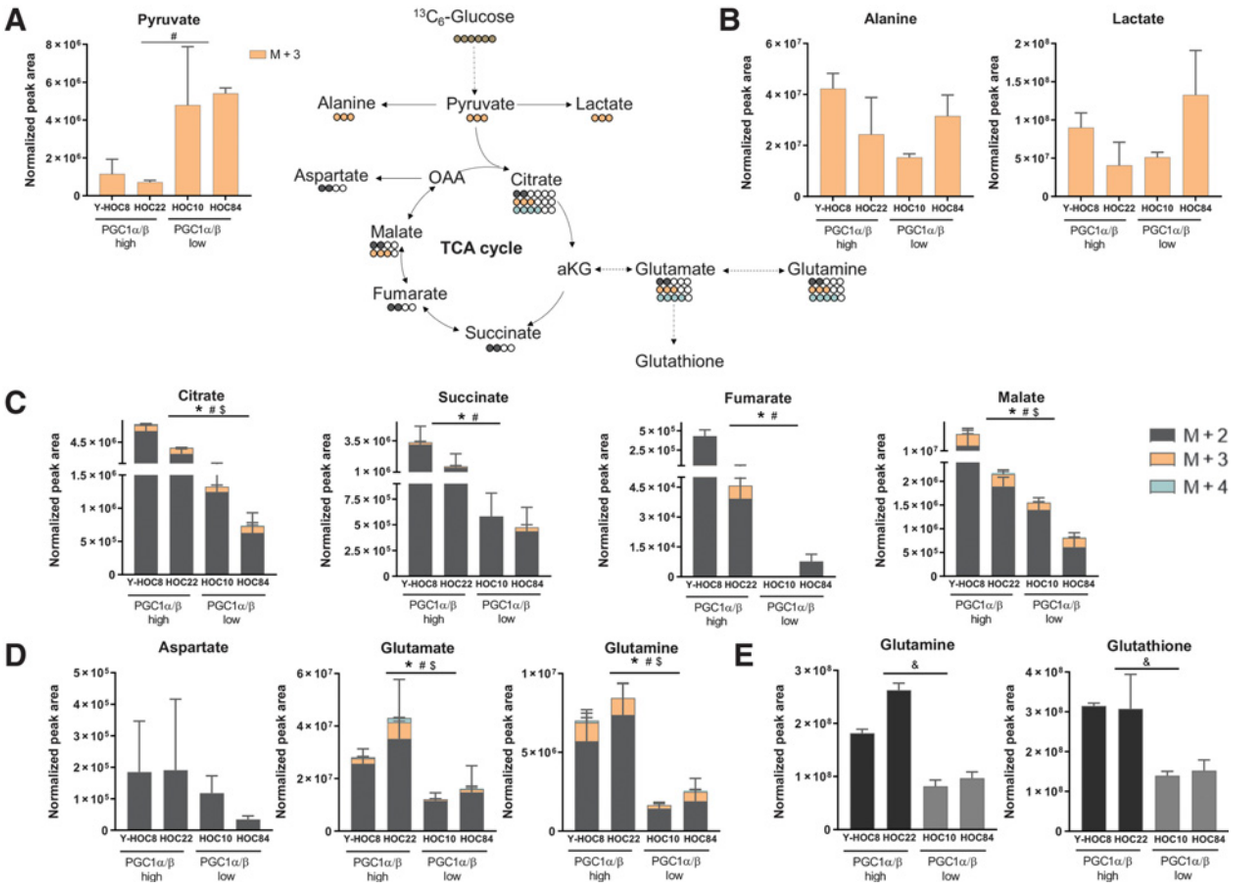

Figure 3.

Mitochondrial functionality is increased in high PGC1α/β-expressing OC-PDX models. The scheme illustrates the fate of glucose ^{13}C atoms in glycolysis, TCA cycle intermediates and TCA-derived metabolites. Two high (Y-HOC8 and HOC22) and two low (HOC10 and HOC84) PGC1α/β-expressing xenografts were injected i.p. with ^{13}C-glucose. **A** and **B,** Isotopolog distribution of pyruvate (M + 3), lactate (M + 3), and alanine (M + 3). **C,** Isotopolog distribution of intracellular intermediates of TCA: citrate, succinate, fumarate, and malate (M + 2, M + 3, M + 4). **D,** Isotopolog distribution of TCA-derived metabolites: aspartate, glutamate, glutamine (M + 2, M + 3, M + 4). **E,** Total intracellular glutamine and glutathione levels. Bar plots represent mean ± SD for each isotopolog fraction. Significant differences ($P < 0.05$) between high (Y-HOC8 and HOC22) and low (HOC10 and HOC84) PGC1α/β-expressing xenografts were analyzed by two-way ANOVA and Tukey multiple test and are marked as *, #, $, and & for M + 2, M + 3, M + 4 and total isotopolog fractions, respectively (three mouse replicates per model). C, carbon.

inhibition, and their high expression characterizes ovarian cancer more sensitive to OXPHOS inhibition.

IACS-010759 inhibits ovarian cancer progression, prolonging the lifespan of mice bearing high PGC1α/β-expressing xenografts

We studied the impact of PGC1α/β stratification on the response to OXPHOS inhibition *in vivo* on three high PGC1α/β expressing OC-PDXs (HOC22, Y-HOC8, and HOC78) and three low PGC1α/β expressing OC-PDXs (HOC76, HOC79, and HOC10). OC-PDXs, growing orthotopically (i.p.), recapitulated the patient's disease, producing ascites and disseminating to the peritoneal organs, thus reproducing the clinical behavior (20, 24). Biological and malignant features (time to progression, production of malignant ascites, or degree of metastasis) did not significantly differ between high and low PGC1α/β expressing OC-PDX (Supplementary Fig. S3).

OC-PDX-bearing mice were treated with 2.5 mg/kg IACS-010759 or vehicle in a maintenance regimen (**Fig. 5**), and the tumor progression and mice survival were evaluated. IACS-010759 was well tolerated, with no toxic effects (Supplementary Fig. S4). The pharmacological inhibition of OXPHOS significantly delayed the progression of the high PGC1α/β expressing OC-PDXs. The necropsy of vehicle-treated mice at terminal sacrifice revealed a significantly high tumor burden, a sign of evident progression of the disease since randomization. In contrast, the abdominal tumor burden of mice undergoing IACS-010759 treatment, recorded at the corresponding median survival times of vehicle-treated mice (days 21, 40, and 34, respectively, for HOC22, Y-HOC8, and HOC78), was significantly lower and did not increase once the treatment started, a sign of disease stabilization (**Fig. 5A**, left). As a consequence, the life of high PGC1α/β OC-PDX-bearing mice was significantly prolonged by 214%, 178%, and 163%, respectively, for HOC22, Y-HOC8, and HOC78 (**Fig. 5A**, right). At autopsy (days 66, 111, and 89.5 median survival times, respectively, for HOC22, Y-HOC8, and HOC78) mice had malignant ascites and abdominal tumor dissemination.

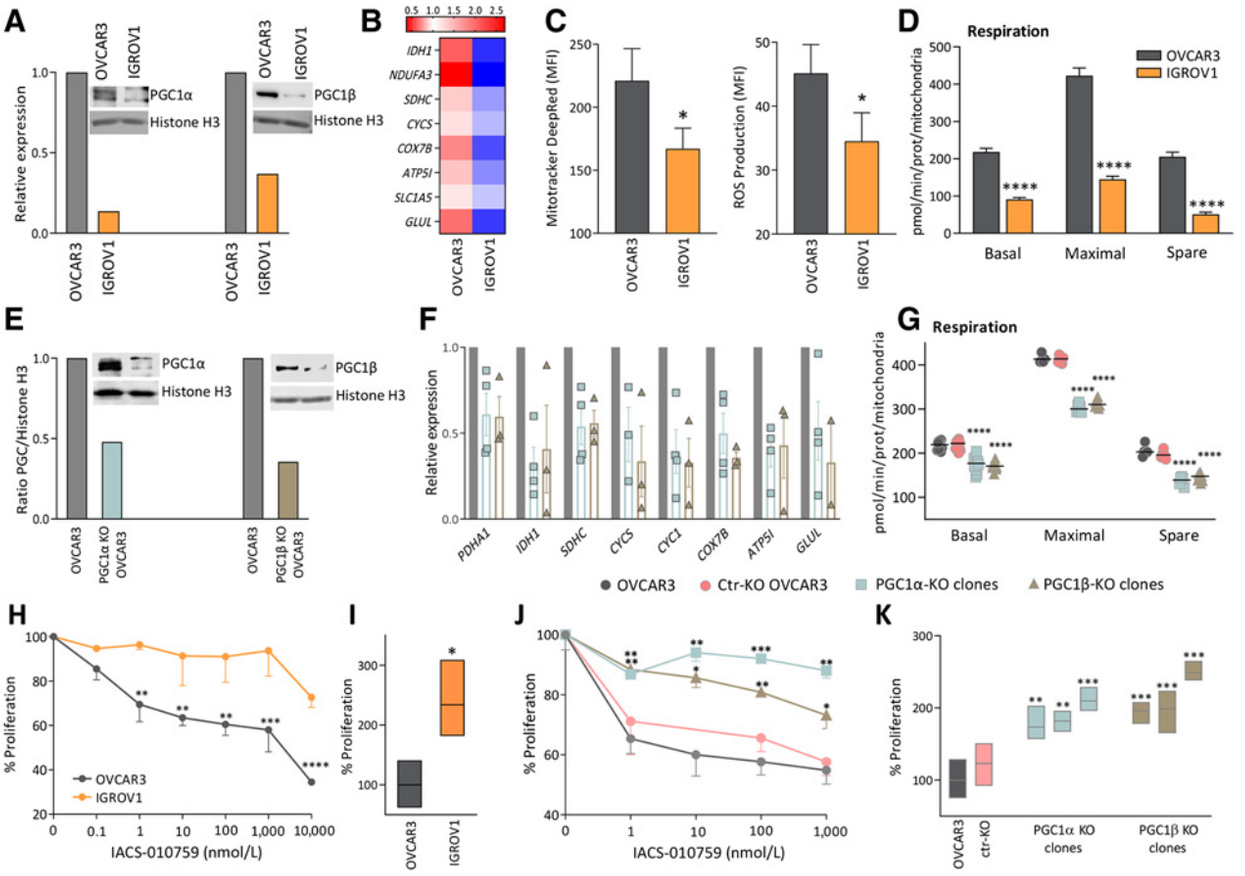

Figure 4.

PGC1α/β regulate OXPHOS metabolism and responsiveness to the OXPHOS inhibitor IACS-010759. **A,** PGC1α and PGC1β transcript expression and proteins in OVCAR3 and IGROV1 cells. **B,** Heatmap of OXPHOS-related gene expression in OVCAR3 compared with IGROV1. **C,** Mean fluorescence intensity of MitoTracker DeepRed and CellROX DeepRed dye (mean ± SD; 3 replicates/cell line). **D,** Basal, maximal OCR (at 0.25 μmol/L FCCP), and spare respiration capacity of OVCAR3 and IGROV1 (mean ± SD). **E,** PGC1α and PGC1β protein levels and representative Western blot in OVCAR3, PGC1α-KO, and PGC1β-KO OVCAR3. **F,** Relative expression of OXPHOS-related genes in OVCAR3 compared with PGC1α-KO OVCAR3 (4 independent clones) and PGC1β-KO OVCAR3 (3 independent clones). **G**, Basal, maximal OCR (at 0.25 μmol/L FCCP) and spare respiration capacity of OVCAR3, ctr-KO OVCAR3, PGC1α-KO, and PGC1β-KO OVCAR3 (the mean line is indicated). **H** and **J,** Dose–response curves to IACS-010759 of OVCAR3 vs. IGROV1 (concentration range, 0.1 nmol/L–10 μmol/L; **H**) and of OVCAR3 vs. ctr-KO, PGC1α-KO, and PGC1β-KO OVCAR3 (concentration range, 1 nmol/L–1 μmol/L; **J**). For each cell line, proliferation of vehicle-treated cells was considered as reference. **I** and **K,** Proliferation of OVCAR3 vs. IGROV1 (**I**) or OVCAR3 vs. ctr-KO OVCAR3 and three independent PGC1α-KO and PGC1β-KO clones (**K**), analyzed by direct cell count after 96 hours exposure to 1,000 nmol/L IACS-010759. The mean proliferation of OVCAR3 in the presence of the drug was considered as reference. *, $P < 0.05$; **, $P < 0.01$; ***, $P < 0.001$; ****, $P < 0.0001$.

Therapeutic benefit on advanced disease was also observed. In the HOC78-bearing mice, IACS-010759 started when the tumor burden was five times higher than in the previous experiment (i.e., 1.8 mL vs. 0.37 mL malignant ascites; Supplementary Fig. S5A and **Fig. 5A**), causing disease stabilization, as observed throughout the third week of treatment (day 46), delaying progression. Thus, the lifespan was increased from 37 days (vehicle-treated mice) to 67 days (IACS-010759-treated mice; Supplementary Fig. S5A).

Conversely, pharmacologic inhibition of OXPHOS did not affect the low PGC1α/β OC-PDXs. IACS-010759 did not inhibit tumor progression of HOC79, HOC76-, and HOC10-bearing mice, and the gain of lifespan was negligible (19% for HOC79 and HOC76 and 7% for HOC10; **Fig. 5B**). IACS-010759 did not give any therapeutic benefit even at the dose of 7.5 mg/kg in HOC79-bearing mice (Supplementary Fig. S5B; a dose three times higher than that in **Fig. 5B**).

Altogether, the *in vitro* and *in vivo* results (**Figs. 4** and **5**) showed that high PGC1α/β levels characterize tumors more addicted to OXPHOS metabolism and more susceptible to OXPHOS inhibition.

IACS-010759 causes mitochondrial swelling and energy crisis in high PGC1α/β OC-PDX

In line with the different response to the drug, IACS-010759 affected mitochondrial structure and energy production in different ways in high and low PGC1α/β OC-PDXs. In the vehicle groups, mitochondria had a normal shape with numerous well-organized intact cristae (**Fig. 6A** and **B**). In the high PGC1α/β HOC22, IACS-010759 significantly reduced the number of mitochondria (2.32 ± 0.17 IACS-010759 vs. 3.35 ± 0.23 vehicle, $P < 0.01$), which suffered severe damage, with partial or total cristolysis and massive swelling, resulting in a 30% increase in mitochondrial volume (0.087 ± 0.006 IACS-010759 vs.

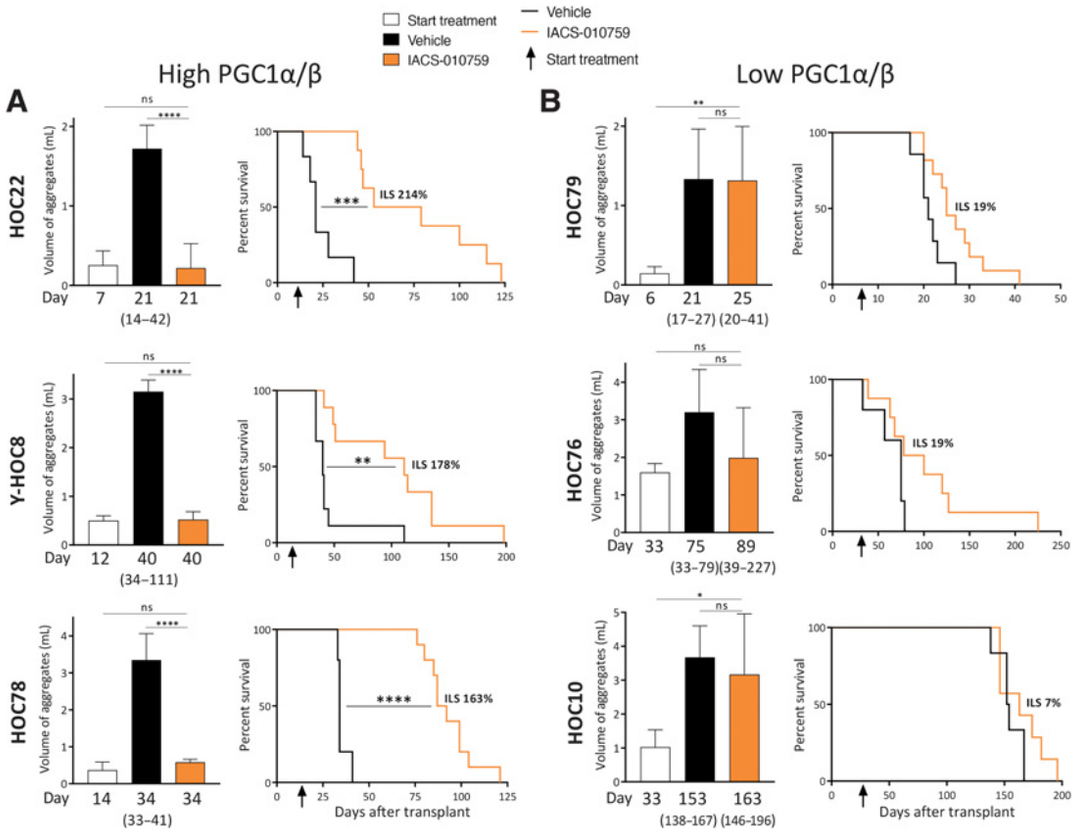

Figure 5.

OXPHOS inhibition affects tumor growth and improves survival of high PGC1α/β OC-PDX-bearing mice. OC-PDXs were transplanted i.p., and mice were randomized at different times after transplant, in relation to their growth: day 7 for HOC22, day 12 for Y-HOC8, day 14 for HOC78, day 6 for HOC79, and day 33 for HOC76 and HOC10. Mice were assigned to receive vehicle or IACS-010759 (2.5 mg/kg) in the maintenance regimen until sacrifice (5–10 mice per group). **A** and **B,** The effect on tumor burden and lifespan of high (**A**) and low (**B**) PGC1α/β-expressing OC-PDX-bearing mice is shown. Left, tumor burden expressed as the volume of cell aggregates in ascites at the start of treatment, at terminal sacrifice and, for responding OC-PDXs, at an interim point corresponding to the median survival time of vehicle-treated mice (mean ± SD; one-way ANOVA multiple comparison). Right, Kaplan–Meier curves showing the effect of IACS-010759 on mice survival. The percentage increment of lifespan (%ILS) is indicated. Log-rank test. ns, not significant; *, $P < 0.05$; **, $P < 0.01$; ***, $P < 0.001$; ****, $P < 0.0001$.

0.067 ± 0.006 vehicle, $P < 0.05$; **Fig. 6A**). In contrast, in the low PGC1α/β HOC10, despite a reduction in mitochondrial abundance (1.38 ± 0.10 IACS-010759 vs. 1.91 ± 0.15 vehicle, $P < 0.01$), mitochondria were not damaged, and their structure was largely unaltered, as well as their volume (1.124 ± 0.0127 IACS-010759 vs. 1.102 ± 0.006, ns; **Fig. 6B**). As a consequence of the mitochondrial alterations in high PGC1α/β expressing OC-PDXs, IACS-010759 led to a significant drop in ATP levels, while ATP production was not significantly affected in the low PGC1α/β OC-PDXs (**Fig. 6C**). These results suggest that high PGC1α/β OC-PDXs depend on OXPHOS as the primary way to produce energy. Therefore, affecting OXPHOS and mitochondria caused an energy crisis, which could not be overcome in the high-OXPHOS OC-PDXs.

Discussion

Deregulated metabolism is a well-documented hallmark of cancer cells (1, 25). Mitochondrial OXPHOS exerts a key role in ensuring the ability to survive and grow in stressful conditions and in microenvironments depleted of nutrients (26). There is evidence suggesting that its targeting could be a promising therapeutic avenue (5, 7–11). However, the potential of this approach has not been investigated in ovarian cancer.

In the present work, we found that OXPHOS inhibition could be effective to manage ovarian cancer progression, and we identified PGC1α and PGC1β as potentially reliable biomarkers predictive of the response.

In orthotopically growing OC-PDX preclinical models, pharmacologic inhibition of OXPHOS significantly constrained malignant progression and prolonged the lifespan of mice bearing tumors with high expression of both PGC1α and PGC1β (PGC1α/β), indicating strong selective antitumor activity. The benefit was also retained in advanced disease, when the drug was given to mice with a heavy tumor burden. These findings may have a valuable impact in patient care considering that we found 25% of ovarian cancer patients' tumors express high levels of PGC1α/β and that patients are frequently diagnosed at advanced stages when the disease has already spread through the peritoneum. The use of PGC1α and PGC1β as biomarkers might permit the selection of patients likely to benefit most from OXPHOS inhibitors. These results are particularly attractive as OXPHOS inhibition is one of the new avenues for cancer treatment with the compendium of inhibitors rapidly expanding (27, 28).

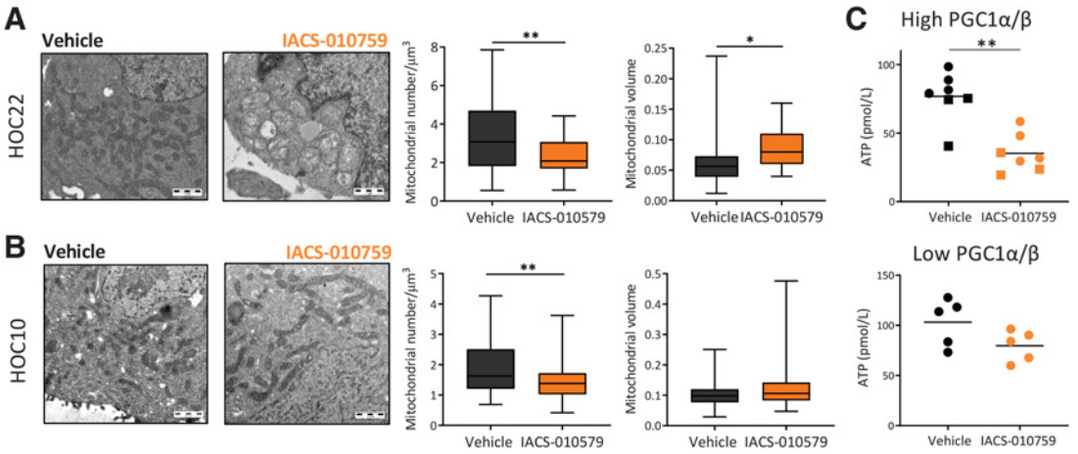

Figure 6.

IACS-010759 affects mitochondria function only in high-expressing PGC1α/β OC-PDX. High PGC1α/β HOC22 and Y-HOC8 and low PGC1α/β HOC10-bearing mice received two doses of vehicle or IACS-010759 (7.5 mg/kg orally) and were euthanized after 3 hours. **A** and **B,** Representative TEM mitochondrial pictures and quantification of mitochondria number and volume from high PGC1α/β HOC22 (**A**) and low PGC1α/β HOC10 (**B**) cell aggregates. Scale bar, 1 µm. **C,** ATP levels in cell aggregates from HOC22, Y-HOC8, and HOC10 ascites. Each point represents one mouse. Unpaired *t* test; *, $P < 0.05$; **, $P < 0.01$.

Notably, OXPHOS inhibition was effective on high PGC1α/β OC-PDX independently from their sensitivity to platinum-based therapy (Supplementary Fig. S6A).

PGC1α and PGC1β are transcriptional coactivators that regulate mitochondrial biogenesis and function in a variety of tissues (12). Their role in cancer is not univocal, but depends closely on tissue- and context-specific determinants (14, 16). We demonstrated that PGC1α/β expression is an inherent trait of each OC-PDX and does not correlate with malignant features, such as tumor burden or metastatic potential. However, their expression distinguishes the tumors with an overactivated OXPHOS gene program, mostly depending on mitochondrial metabolism as primary energy source. PGC1α/β raise the mitochondrial content and functions—respiration and TCA cycling—and enhance antioxidant defense. Most importantly, we showed that high PGC1α/β levels could generate metabolic vulnerabilities, boosting the sensitivity of tumors to OXPHOS inhibitors. IACS-010759 affected the *in vitro* proliferation of high PGC1α/β OVCAR3 but not of PGC1α– and PGC1β–silenced OVCAR3 cells, as well as low PGC1α/β IGROV1. *In vivo*, we confirmed that IACS-010759 selectively induced mitochondrial damage in high PGC1α/β OC-PDX, which were then unable to overcome the energy crisis and ATP depletion, impairing the tumor progression. We demonstrate that mitochondria of high and low PGC1α/β tumors present basal structural differences and different expression of proteins involved in cristae organization and the mitochondrial transport system (Supplementary Tables S2 and S3), which can contribute to the enhanced susceptibility to OXPHOS inhibitors owing to higher or lower target access in the respiratory chain. High and low PGC1α/β OC-PDXs shared metabolic features and drug sensitivity with the high- and low-OXPHOS ovarian cancer cell subsets, recently described in Gentric at al., where high-OXPHOS cells showed higher mitochondrial activity and enhanced sensitivity to the OXPHOS inhibitor metformin (29).

Analyzing public gene expression data (GSE64497 dataset; ref. 30), we found that SK-MEL-5 melanoma cells—highly responsive to IACS-010759 (31)—had higher PGC1α/β expression than the low responsive A375 cells. Accordingly, high expression characterized a subset of melanoma cells with greater mitochondrial capacity (32), indicating that high expression of PGC1α/β might be useful to define OXPHOS dependency and predict the responsiveness to OXPHOS inhibitors also in tumor types other than ovarian cancer.

It has also been demonstrated that BRAF inhibitors induce OXPHOS dependence in melanoma, through PGC1α upregulation (33). Inhibition of OXPHOS with phenformin synergizes with BRAF inhibitors and induces tumor regression (34). This suggests that it is worth exploiting OXPHOS inhibitors for the treatment of high PGC1α/β tumors in combination therapies. When tested in combination with platinum (DDP) in a sequential schedule, IACS-010759 further prolonged mouse lifespan compared with the monotherapy, giving a survival advantage (Supplementary Fig. S6B). Thus, the combination between standard chemotherapy and OXPHOS inhibitors offer a suitable therapeutic option and call for more investigation. Recently, ovarian cancer therapy has been implemented by the introduction of PARP inhibitors, highly effective in homologous recombination–deficient (HRD) tumors (35). A recent study postulated an association between HRD and increased oxidative metabolism (36), that we also noticed in our OC-PDX cohort, where 78% BRCA-deficient OC-PDXs had high PGC1α/β against only 7% BRCA-proficient OC-PDX (**Fig. 1D**). The link between HRD and OXPHOS opens a new window for exploring the role of metabolism in the response to PARP inhibitors and lays the grounds for combinations with PARP and OXPHOS inhibitors.

Appropriate selection of patients is a major challenge in translating preclinically effective drugs to clinical trials. This may be particularly relevant for OXPHOS inhibitors since mitochondria-targeting agents can cause substantial side effects. To date, most of the available OXPHOS inhibitors target the complex I of ETC, but their use is limited by the elevated toxicity due to their off-target effects or poor biodistribution (37). Many efforts are ongoing to design more specific inhibitors (including IACS-010759 used in the present work) that can overcome these problems. Another limit for drugging mitochondrial OXPHOS is the incomplete understanding of the tumor contexts where OXPHOS is essential and the lack of tools to identify tumor metabolic vulnerability. Our work shows that PGC1/β expression might be exploited to predict the responsiveness to OXPHOS inhibitors, permitting patient stratification. We found that, analogous

to OC-PDXs, high PGC1α/β expression in patients' specimens did not correlate with the clinical features, progression-free or overall survival, but was significantly associated with an OXPHOS gene program and could therefore distinguish tumors mostly relying on mitochondrial metabolism. Our results point to these tumors as potential clinical responders for treatments targeting OXPHOS and endorse the use of PGC1α and PGC1β as biomarkers, although further studies are needed for their validation and for designing appropriate screening tests.

Authors' Disclosures

F. Chiaradonna reports grants from government agency outside the submitted work. G.F. Draetta reports personal fees from Frontier Medicines and Metabomed outside the submitted work. J.R. Marszalek reports a patent for WO 2014/031928 A2 issued to UT MD Anderson, and IACS-010759 development was supported in part by the MD Anderson Moon Shot program and through a collaboration between the IACS and TRACTION platforms. No disclosures were reported by the other authors.

Authors' Contributions

C. Ghilardi: Conceptualization, investigation, writing–original draft. **C. Moreira-Barbosa:** Investigation. **L. Brunelli:** Investigation, methodology. **P. Ostano:** Data curation, formal analysis. **N. Panini:** Investigation. **M. Lupi:** Investigation. **A. Anastasia:** Investigation. **F. Fiordaliso:** Investigation. **M. Salio:** Investigation. **L. Formenti:** Investigation. **M. Russo:** Investigation. **E. Arrigoni:** Investigation. **F. Chiaradonna:** Investigation. **G. Chiorino:** Data curation, formal analysis. **G.Draetta:** Resources, writing–review and editing. **J.R. Marszalek:** Resources, writing–review and editing. **C.P. Vellano:** Resources, writing–review and editing. **R. Pastorelli:** Supervision, writing–review and editing. **M. Bani:** Supervision, writing–review and editing. **A. Decio:** Funding acquisition, investigation, project administration. **R. Giavazzi:** Supervision, funding acquisition, writing–review and editing.

Acknowledgments

Research reported in this publication was supported by the Italian Association for Cancer Research (AIRC IG2019 ID 23520 to R. Giavazzi) and Fondazione Cariplo (Grant n 2017-0896 to A. Decio). The authors thank Fundação para a Ciência e a Tecnologia for PhD grant to C. Moreira-Barbosa (FCT, grant PD/BD/135451/2017). Thanks to Prof. Nico Mitro and Dr. Matteo Audano (University of Milan, Department of Pharmacologic and Biomolecular Sciences) for the courtesy of Clark Electrode and helpful feedback.

The costs of publication of this article were defrayed in part by the payment of page charges. This article must therefore be hereby marked *advertisement* in accordance with 18 U.S.C. Section 1734 solely to indicate this fact.

Received April 19, 2021; revised October 11, 2021; accepted February 2, 2022; published first February 7, 2022.

References

1. Hanahan D, Weinberg RA. Hallmarks of cancer: the next generation. Cell 2011; 144:646–74.
2. Zheng J. Energy metabolism of cancer: glycolysis versus oxidative phosphorylation (review). Oncol Lett 2012;4:1151–7.
3. Reznik E, Miller ML, Şenbabaoğlu Y, Riaz N, Sarungbam J, Tickoo SK, et al. Mitochondrial DNA copy number variation across human cancers. Elife 2016;5: e10769.
4. Wang Y, Liu VWS, Xue WC, Cheung ANY, Ngan HYS. Association of decreased mitochondrial DNA content with ovarian cancer progression. Br J Cancer 2006; 95:1087–91.
5. Yang L, Moss T, Mangala LS, Marini J, Zhao H, Wahlig S, et al. Metabolic shifts toward glutamine regulate tumor growth, invasion and bioenergetics in ovarian cancer. Mol Syst Biol 2014;10:728.
6. Sotgia F, Lisanti MP. Mitochondrial mRNA transcripts predict overall survival, tumor recurrence and progression in serous ovarian cancer: companion diagnostics for cancer therapy. Oncotarget 2017;8:66925–39.
7. Bosc C, Selak MA, Sarry J-E. Resistance is futile: Targeting mitochondrial energetics and metabolism to overcome drug resistance in cancer treatment. Cell Metab 2017;26:705–7.
8. Emmings E, Mullany S, Chang Z, Landen CN, Linder S, Bazzaro M. Targeting mitochondria for treatment of chemoresistant ovarian cancer. Int J Mol Sci 2019; 20:229.
9. Matassa DS, Amoroso MR, Lu H, Avolio R, Arzeni D, Procaccini C, et al. Oxidative metabolism drives inflammation-induced platinum resistance in human ovarian cancer. Cell Death Differ 2016;23:1542–54.
10. Pastò A, Pagotto A, Pilotto G, De Paoli A, De Salvo GL, Baldoni A, et al. Resistance to glucose starvation as metabolic trait of platinum-resistant human epithelial ovarian cancer cells. Oncotarget 2017;8:6433–45.
11. Pastò A, Bellio C, Pilotto G, Ciminale V, Silic-Benussi M, Guzzo G, et al. Cancer stem cells from epithelial ovarian cancer patients privilege oxidative phosphorylation, and resist glucose deprivation. Oncotarget 2014;5:4305–19.
12. Lin J, Handschin C, Spiegelman BM. Metabolic control through the PGC-1 family of transcription coactivators. Cell Metab 2005;1:361–70.
13. Villena JA. New insights into PGC-1 coactivators: redefining their role in the regulation of mitochondrial function and beyond. FEBS J 2015;282:647–72.
14. Luo C, Widlund HR, Puigserver P. PGC-1 coactivators: shepherding the mitochondrial biogenesis of tumors. Trends Cancer 2016;2:619–31.
15. LeBleu VS, O'Connell JT, Gonzalez Herrera KN, Wikman H, Pantel K, Haigis MC, et al. PGC-1α mediates mitochondrial biogenesis and oxidative phosphorylation in cancer cells to promote metastasis. Nat Cell Biol 2014;16:992–1003,1–15.
16. Gravel S-P. Deciphering the dichotomous effects of PGC-1α on tumorigenesis and metastasis. Front Oncol 2018;8:75.
17. Molina JR, Sun Y, Protopopova M, Gera S, Bandi M, Bristow C, et al. An inhibitor of oxidative phosphorylation exploits cancer vulnerability. Nat Med 2018;24: 1036–46.
18. Workman P, Aboagye EO, Balkwill F, Balmain A, Bruder G, Chaplin DJ, et al. Guidelines for the welfare and use of animals in cancer research. Br J Cancer 2010;102:1555–77.
19. Decio A, Cesca M, Bizzaro F, Porcu L, Bettolini R, Ubezio P, et al. Cediranib combined with chemotherapy reduces tumor dissemination and prolongs the survival of mice bearing patient-derived ovarian cancer xenografts with different responsiveness to cisplatin. Clin Exp Metastasis 2015;32:647–58.
20. Ricci F, Bizzaro F, Cesca M, Guffanti F, Ganzinelli M, Decio A, et al. Patient-derived ovarian tumor xenografts recapitulate human clinicopathology and genetic alterations. Cancer Res 2014;74:6980–90.
21. Caiola E, Colombo M, Sestito G, Lupi M, Marabese M, Pastorelli R, et al. Glutaminase inhibition on NSCLC depends on extracellular alanine exploitation. Cells. 2020;9:1766.
22. Terao M, Goracci L, Celestini V, Kurosaki M, Bolis M, Di Veroli A, et al. Role of mitochondria and cardiolipins in growth inhibition of breast cancer cells by retinoic acid. J Exp Clin Cancer Res 2019;38:436.
23. Pils D, Hager G, Tong D, Aust S, Heinze G, Kohl M, et al. Validating the impact of a molecular subtype in ovarian cancer on outcomes: a study of the OVCAD Consortium. Cancer Sci 2012;103:1334–41.
24. Oliva P, Decio A, Castiglioni V, Bassi A, Pesenti E, Cesca M, et al. Cisplatin plus paclitaxel and maintenance of bevacizumab on tumour progression, dissemination, and survival of ovarian carcinoma xenograft models. Br J Cancer 2012; 107:360–9.
25. Pavlova NN, Thompson CB. The emerging hallmarks of cancer metabolism. Cell Metab 2016;23:27–47.
26. Viale A, Corti D, Draetta GF. Tumors and mitochondrial respiration: a neglected connection. Cancer Res 2015;75:3685–6.
27. Sica V, Bravo-San Pedro JM, Stoll G, Kroemer G. Oxidative phosphorylation as a potential therapeutic target for cancer therapy. Int J Cancer 2020;146:10–7.
28. Nayak AP, Kapur A, Barroilhet L, Patankar MS. Oxidative phosphorylation: a target for novel therapeutic strategies against ovarian cancer. Cancers 2018; 10:337.
29. Gentric G, Kieffer Y, Mieulet V, Goundiam O, Bonneau C, Nemati F, et al. PML-regulated mitochondrial metabolism enhances chemosensitivity in human ovarian cancers. Cell Metab 2019;29:156–73.

30. Ploper D, Taelman VF, Robert L, Perez BS, Titz B, Chen H-W, et al. MITF drives endolysosomal biogenesis and potentiates Wnt signaling in melanoma cells. Proc Natl Acad Sci U S A 2015;112:E420–429.
31. Vashisht Gopal YN, Gammon S, Prasad R, Knighton B, Pisaneschi F, Roszik J, et al. A novel mitochondrial inhibitor blocks MAPK pathway and overcomes MAPK inhibitor resistance in melanoma. Clin Cancer Res 2019;25:6429–42.
32. Vazquez F, Lim J-H, Chim H, Bhalla K, Girnun G, Pierce K, et al. PGC1α expression defines a subset of human melanoma tumors with increased mitochondrial capacity and resistance to oxidative stress. Cancer Cell 2013; 23:287–301.
33. Haq R, Shoag J, Andreu-Perez P, Yokoyama S, Edelman H, Rowe GC, et al. Oncogenic BRAF regulates oxidative metabolism via PGC1α and MITF. Cancer Cell 2013;23:302–15.
34. Yuan P, Ito K, Perez-Lorenzo R, Del Guzzo C, Lee JH, Shen C-H, et al. Phenformin enhances the therapeutic benefit of BRAF(V600E) inhibition in melanoma. Proc Natl Acad Sci U S A 2013;110:18226–31.
35. Moore K, Colombo N, Scambia G, Kim B-G, Oaknin A, Friedlander M, et al. Maintenance Olaparib in patients with newly diagnosed advanced ovarian cancer. N Engl J Med 2018;379:2495–505.
36. Lahiguera Á, Hyroššová P, Figueras A, Garzón D, Moreno R, Soto-Cerrato V, et al. Tumors defective in homologous recombination rely on oxidative metabolism: relevance to treatments with PARP inhibitors. EMBO Mol Med 2020;12: e11217.
37. Ashton TM, McKenna WG, Kunz-Schughart LA, Higgins GS. Oxidative phosphorylation as an emerging target in cancer therapy. Clin Cancer Res 2018;24: 2482–90.